Mechanics of Materials 211 (2025) 105506

Contents lists available at ScienceDirect

Mechanics of Materials

journal homepage: www.elsevier.com/locate/mechmat

Research paper

Inversion of the thermomechanical response in nitinol under cyclic loading: an analytical interpretation based on the thermoelastic effect theory

V. Pinto [a,b,1], S. Di Leonardo [a,b,1], G. Pitarresi [a,*], G. Burriesci [a,b,c]

[a] Università degli Studi di Palermo - Engineering Department, Viale delle Scienze, 90128, Palermo, Italy
[b] Ri.MED Foundation, Bioengineering Group, Viale delle Scienze, Palermo, 90128, Italy
[c] UCL Mechanical Engineering, University College London, Torrington Pl, London, WC1E 7JE, UK

ARTICLE INFO

Handling Editor: Jean-F Molinari

Keywords:
Superelastic nitinol
Austenite
Thermomechanical coupling
Thermoelastic stress analysis
Thermoelastic effect
Infrared thermography

ABSTRACT

The superelastic behaviour of nitinol is crucial for the design of collapsible and self-expanding cardiovascular implants. Once these are expanded into the host anatomy, the material is predominantly in the austenitic configuration in the majority of the structure, and the cyclic loads acting on the devices are primarily due to small blood pressure variations occurring during the cardiac cycle. Nevertheless, only very few studies have explored the temperature evolution during small cyclic loading of nitinol in a stable austenitic state, reporting an unusual response, where the thermoelastic signal is in phase with the sinusoidal loading wave, rendering the common fundamental law of the thermoelastic effect inapplicable. In this study, infrared thermography (IRT) was employed to investigate the thermomechanical behaviour of an austenitic nitinol specimen under cyclic sinusoidal loading, with increasing amplitude and average strain values. An inversion of the thermomechanical response of nitinol was observed experimentally and explained analytically adopting the higher-order thermoelastic theory. The understanding of the austenitic temperature modulation with the local level of stress allowed to define an IRT approach suitable to quantify the stress levels, knowing the material thermal response and the ratio between mean and amplitude of the applied load.

1. Introduction

Nitinol is a nearly equi-atomic Nickel-Titanium alloy that presents two possible crystalline structures: austenite, stable at high temperatures and low stress, and martensite, stable at lower temperatures and high stress. The transformation between these two phases, which can be induced by the stress level or by temperature changes, confers the material its peculiar superelastic or shape memory behaviour. Unloaded superelastic nitinol is in the austenitic configuration. When subjected to a load, austenite follows an elastic, approximately linear, behaviour up to a stress level that initiates a stress-induced martensite transformation (SIMT). After that, the stress keeps about stable up to completion of the phase transformation, which occurs at strain levels of about 7–8 %. Once the material is completely transformed, if the load is increased further, martensite follows an elastic about linear behaviour up to yielding. Below this stage, the transformation is reversible: upon unloading, martensite retransforms into austenite along a plateau at lower stress than that associated with the transformation during loading, and eventually recovers the whole deformation (Lagoudas, 2008; Zheng et al., 2016).

This property is widely exploited in the support structures used for minimally invasive biomedical devices, where the superelastic behaviour is the most essential feature in self-expanding cardiovascular implants, including angioplasty stents, stent grafts for endovascular aneurysm repair and transcatheter heart valves (Petrini and Migliavacca, 2011; Wadood, 2016). These devices are collapsed into a catheter, that is delivered to the anatomical position through the vasculature, and then let to re-expand to its operating configuration, thus avoiding surgery and the related complications. The support components typically consist of cellular structures composed of interconnected nitinol struts, that deform under the effect of elastic flexural deformation and pseudo-plastic hinges forming at the strut joints (Wolcott, 1990). When the device is loaded into the delivery system, these hinges experience SIMT, undergoing large superelastic deformations, which are recovered when the device self-expands at the end of the implant (Tzamtzis et al., 2013). A reliable experimental stress

* Corresponding author.
E-mail address: giuseppe.pitarresi@unipa.it (G. Pitarresi).
[1] The first two authors contributed equally to this work.

https://doi.org/10.1016/j.mechmat.2025.105506
Received 27 February 2025; Received in revised form 29 August 2025; Accepted 20 September 2025
Available online 22 September 2025

analysis method suitable for the study of self-expanding devices operating in their implanted configuration would be essential to assess and optimise their design and efficacy. In this context, infrared thermography (IRT) has been established as one of the most effective techniques for non-contact and full-field temperature measurements. The technique relates the temperature of an object to its electromagnetic radiation in the infrared field. However, IRT applications to the analysis of nitinol have been mostly qualitative and limited to the detection of the localised latent heat in the phase transformation front, well-known as elasto-caloric effect (Churchill et al., 2010; Pieczyska et al., 2013). In fact, as the material releases heat in the stress induced transformation from austenite to martensite and absorbs heat during the reverse phase transformation, during the crystal rearrangement, it expresses a marked signature on the temperature map which is clearly detected by infrared cameras. This phenomenon is accompanied by significant changes in the superelastic behaviour, which result in fatigue failure after relatively few deformation cycles (Bonsignore et al., 2019; Furgiuele et al., 2020; Soul and Yawny, 2017; Tušek et al., 2018; Xie et al., 2016; Yin et al., 2021).

The elasto-caloric effect has been extensively investigated in the literature (Song et al., 2026; Xiao and Jiang, 2022; Yu et al., 2015, 2022; Zhang et al., 2022, 2024), exploring phenomena such as the crystal reorientation, the thermomechanical instability during localised transformation at different temperatures and uncharacteristic phase transformation phenomena. While these studies have provided significant insights into the fundamental aspects of nitinol thermomechanical behaviour, they overlook the material thermoelastic response, which is particularly relevant in practical applications, where the material remains predominantly austenitic. In fact, in the case of nitinol cardiovascular implants, the phase transformation is only experienced during the crimping and delivery phases, when the material at the hinge regions undergoes a complete superelastic transformation and, therefore, is not associated with fatigue. Once the device is implanted, the material returns to the austenitic configuration (with the potential exception of small localised martensitic regions) (Berti et al., 2021) and is subjected to the small strain amplitudes produced by the blood pressure fluctuations occurring during the cardiac cycle. For this condition, high-cycle structural fatigue failure is expected (Cao et al., 2020; Launey et al., 2023; Mitchell et al., 2019; Senthilnathan et al., 2019). Despite this representing the most relevant form of load experienced by high risk transcatheter medical devices, only very few studies have investigated the temperature evolution of nitinol in a stable austenitic configuration during small cyclic loading (Ahadi et al., 2019; Di Leonardo et al., 2021; Eaton-Evans et al., 2006; Pinto et al., 2025). This is justified by the unusual response observed in these tests, which is characterised by a thermoelastic signal in phase with the loading (Eaton-Evans et al., 2006, 2008). The practical observations of nitinol heating under tension demonstrate a potential limitation of the fundamental law of the thermoelastic effect and conventional thermoelastic stress analysis (TSA).

The hypothesis of this work is that the unusual thermomechanical behaviour of austenitic nitinol under cyclic sinusoidal loading can be explained and interpreted by adopting the *higher-order thermoelastic theory* proposed by (Wong et al., 1987), with the aim to expand the application of TSA to the assessment of austenitic nitinol.

Specifically, TSA was applied to study the thermomechanical response of an austenitic nitinol specimen under cyclic sinusoidal loading at increasing values of the amplitude and average strain. The significance of this work lies in demonstrating that, despite the use of the common thermoelastic stress analysis leads to largely incorrect predictions of the stress state, the higher-order thermoelastic theory allows for the accurate determination of the stress state. This analytical explanation of the thermomechanical behaviour observed experimentally aims to implement a material characterisation approach more suitable for real medical applications.

2. Materials and methods

2.1. Experimental setup

2.1.1. Differential scanning calorimetry

A sample of 38.6 mg was extracted from a sheet of superelastic nitinol 0.4 mm thick and used to determine the phase transformation temperatures by differential scanning calorimetry (DSC) analysis. The test was performed on a DSC 131 system (Setaram, Caluire-et-Cuire, France) applying a sequence of thermal ramps in the range −40 °C–200 °C, at a rate of 5 °C/min. Phase transformation temperatures were obtained from the heat flow peaks in compliance with the standard ASTM F2004-03 (2018).

2.1.2. Mechanical testing

A nitinol strip of dimensions 10 mm × 100 mm was cut from the same sheet characterised by DSC, by means of electrical discharge machining, so as to minimise the residual stresses introduced by the cutting process. One face of the specimen was painted with matte black dye, to enhance infrared emission and reduce the effects of environmental reflection in the IRT analysis, and the other was painted with matte black speckle on a matte white background, for digital image correlation (DIC) analysis. The strip was gripped on an electrodynamic testing machine BOSE Electroforce 3550 (TA Instruments, UK), leaving a gauge length of 67.5 mm, and tested at room temperature ($T_0 = 290.66$ K). The temperature of the black painted face of the specimen was acquired with a cooled sensor FLIR X6540SC thermal camera (Teledyne FLIR LLC, UK), while the other face was photographed during the deformations with a reflex Nikon D5100 camera (Nikon Corporation, Tokyo, Japan) with a ring led light mounted to the objective Micro-Nikkor 105 mm f/2.8 (experimental set-up in Fig. 1a).

The strip was initially characterised through a quasi-static tensile test in displacement control at a speed of 0.50 mm/min, reaching a maximum displacement of 0.44 mm (0.7 % deformation).

Subsequently, the sample was subjected to a series of 5 traction-traction sinusoidal loadings, applying for each test a sequence of 2 cycles at a frequency of 0.02 Hz, followed by 60 cycles at a frequency of 1 Hz. Test were performed in displacement control with maximum and minimum target displacements of the moving crosshead equal to 0.1 mm and 0.15 mm for test 1; to 0.1 mm and 0.2 mm for test 2; to 0.1 mm and 0.25 mm for test 3; to 0.1 mm and 0.3 mm for test 4; and to 0.1 mm and 0.35 mm for test 5. However, some departure from the target displacements was observed at the higher frequency (1 Hz), with a reduction in the amplitude of the sinusoidal loading (applied displacement in Fig. 1b).

Deformation of quasi-static test and cycles at 0.02 Hz was acquired with the camera at 4 s intervals, for DIC analysis. Specimen surface temperature was acquired during the cycles at 1 Hz with the thermal camera, with acquisition sampling rate of 50 frames per second.

DIC analysis was performed by using Ncorr (Blaber et al., 2015), a Matlab (MathWorks, USA) open-source software. The software subdivides the reference image into subsets and tracks the subset displacements in the following images by means of correlation function. Subsequently, the displacement gradients are used to evaluate the full field strains by selecting a specific number of subsets to reduce signal noise. Tests were analysed by setting a subset radius of 15 px, spaced every 7 px, and 3 subset spacings for strain calculation, with a magnification factor of the camera pictures of 0.0167 mm/px. Resulting strain maps were averaged over the specimen gauge length surface, obtaining the mean specimen deformation. DIC strains were used to obtain stress-strain curves. Stress was evaluated as force divided by initial cross-section. Full-field thermograms were averaged over the gauge length surface, obtaining a temperature signal over time for each test. To better identify temperature peak values, the thermal signal was smoothed out by applying the *smoothdata* function available in Matlab, imposing a robust quadratic regression. Mean peak values were

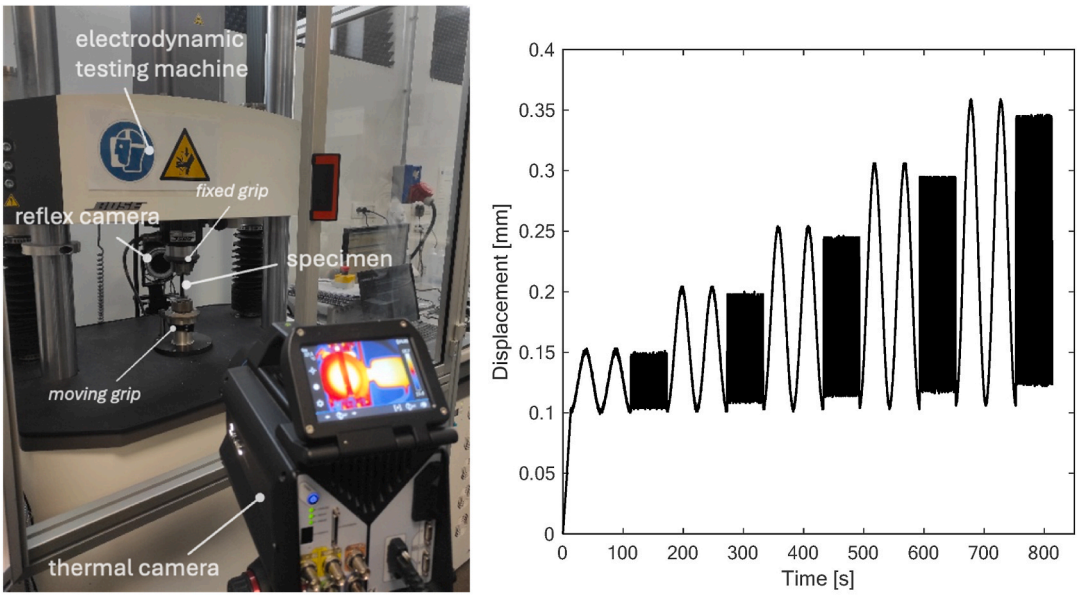

(a) (b)

Fig. 1. a) Experimental set-up; b) displacement vs time curve.

evaluated as the average of five consecutive cycles.

2.2. Nitinol thermomechanical modelling

2.2.1. Theoretical background

TSA exploits the thermoelastic effect (i.e. the temperature variations that occur due to elastic deformations induced by applied loads) to extract information on the state of stress in a material. For the case of nitinol, the thermomechanical behaviour has commonly been modelled by applying the theory of thermodynamics for solid systems (Chrysochoos, 2012a; Chrysochoos et al., 1996), based on the first and second principles of thermodynamics, and a set of state variables which include the temperature T, the strain tensor ε_{ij} and other internal state variables included into a vector $\boldsymbol{x}$. These latter serve to describe the energetic implications of mechanically induced changes of material states. In the case of nitinol, such internal state variables have, for instance, been proposed to consider the micro-lattice phase status and its changes (Peyroux et al., 1998). By combining the first and second principles of thermodynamics and introducing the Helmholtz free energy (F), it is possible to obtain the local energy balance in the form of a heat diffusion law, as follows (Lemaitre et al., 1993):

$$\rho\, c_v\, \dot{T} - k\, \nabla^2 T = D_m + T\rho \frac{\partial^2 F}{\partial T \partial \varepsilon_{ij}} \dot{\varepsilon}_{ij} + T\, \rho \frac{\partial^2 F}{\partial T \partial \boldsymbol{x}} \dot{\boldsymbol{x}} + q_s \tag{1}$$

where ρ is the material density, c_v the specific heat at constant volume, k the scalar isotropic heat conductivity, D_m the intrinsic dissipation, and q_s quantifies the external heat sources.

The first and second terms of the left-hand side of Equation (1) describes the heat stored/released by conduction, considering an isotropic Fourier heat conduction law. The right-hand side provides the deformation-induced heat sources (first three terms) and the heat supply from the environment. The second term is related to the thermoelastic effect heat source. Under linear reversible elastic straining conditions, the derivative of the potential F with respect to strain provides the following thermoelastic state law (Lemaitre et al., 1993):

$$\sigma_{ij} = \rho \frac{\partial F}{\partial \varepsilon_{ij}} \tag{2}$$

where σ_{ij} is the Cauchy stress tensor associated with the elastic strain.

Under linear elastic cyclic straining, the intrinsic dissipation in Equation (1) can be considered negligible compared to the thermoelastic contribution. The third term can be associated with the latent heat of the phase transformation and matter changes (Chrysochoos, 2012b; Lemaitre et al., 1993). If the loading amplitude is sufficiently small to be included within a purely elastic material response (it does not activate the austenite-martensite phase transformation), it is possible to assume $\dot{\boldsymbol{x}} = 0$. Finally, when the material undergoes cyclic loading at a sufficiently high frequency, it can be assumed that the transformation is adiabatic (i.e. no internal heat conduction arises), so that the second term on the left-hand side of Equation (1) becomes negligible. Adiabatic conditions also imply that the term q_S, considering heat flux from and to the environment, is negligible.

All previous simplifications allow rewriting Equation (1) as follows (Pitarresi and Patterson, 2003):

$$\rho\, c_v \frac{\dot{T}}{T} = \frac{\partial \sigma_{ij}}{\partial T} \dot{\varepsilon}_{ij}. \tag{3}$$

Further details about the assumptions and derivations leading to this expression, starting from Equation (1), are well described in Lemaitre et al. (1993) and Pitarresi and Patterson (2003).

Integrating over a finite time, and assuming that temperature and strain changes are small compared to the initial values T_o and $(\dot{\varepsilon}_{ij})_0$, Equation (3) can also be written as:

$$\Delta T = -T_0 \frac{1}{\rho\, c_v} \cdot \frac{\partial \sigma_{ij}}{\partial T} \Delta \varepsilon_{ij}. \tag{4}$$

The first-order thermoelastic law is based on the assumption that all elastic constants have a negligible dependence on temperature changes. This is an acceptable assumption for most materials. In this case, Equation (4) can be further simplified as follows:

$$\Delta T = -T_0 \frac{\alpha}{\rho\, c_v} \cdot \frac{E}{1-2\nu} \Delta \varepsilon_{kk} \approx -T_0 \frac{\alpha}{\rho\, c_v} \Delta \sigma_{kk} \tag{5}$$

where E is the Young's modulus, ν is the Poisson's ratio and α is the coefficient of thermal expansion.

This is commonly known as the *fundamental law of the thermoelastic*

effect, and expresses the temperature variation (ΔT) experienced during loading as a linear function of the strain or stress first invariant ($\Delta\varepsilon_{kk}$ and $\Delta\sigma_{kk}$, respectively). The latter expression, written in terms of $\Delta\sigma_{kk}$, assumes that due to the small value of α, the strain variation due to temperature change is negligible.

As described by Equation (5), standard materials heat up when subjected to a compressive load (negative volume variation) and cool down when subjected to a tensile load (positive volume variation). Nevertheless, as mentioned above, this law appears inadequate to explain the thermal response observed in nitinol tests, which is reported to follow an opposite relationship between ΔT and the stress/strain invariant (Ahadi et al., 2019; Di Leonardo et al., 2021; Eaton-Evans et al., 2006).

A *higher-order thermoelastic law* was derived by Wong et al. (1987), where the dependence of the material parameters from T is taken into account:

$$\rho c_v \frac{\dot{T}}{T} = -\left[\alpha + \left(\frac{\nu}{E^2}\cdot\frac{\partial E}{\partial T} - \frac{1}{E}\cdot\frac{\partial \nu}{\partial T}\right)\sigma_I\right]\dot{\sigma}_I + \left[\frac{(1+\nu)}{E^2}\cdot\frac{\partial E}{\partial T} - \frac{1}{E}\cdot\frac{\partial \nu}{\partial T}\right]\sigma_i\,\dot{\sigma}_i \tag{6}$$

with $\sigma_i = \sigma_1;\sigma_2;\sigma_3$ corresponding to the principal stress components and $\sigma_I = \sigma_1 + \sigma_2 + \sigma_3$ to the first stress invariant.

If a one-dimensional stress field is considered: $\sigma_I \equiv \sigma_i = \sigma_1 = \sigma$ ($\sigma_2 = \sigma_3 = 0$), and the terms including the Poisson's ratio cancel out, Equation (6) simplifies into:

$$\rho\, c_v \frac{\dot{T}}{T} = -\left[\alpha - \frac{1}{E^2}\cdot\frac{\partial E}{\partial T}\sigma\right]\dot{\sigma}. \tag{7}$$

It is worth observing that the stress state experienced by nitinol in medical devices is mostly associated with bending moment acting on struts, and is therefore about uniaxial.

To achieve adiabatic conditions, TSA usually applies cyclic loads. Considering a sinusoidal tensile load in the form $\sigma = \sigma_m + \sigma_a \sin(\omega t + \varphi)$, where ω is the frequency and φ is the phase, assumed equal to zero, Equation (7) becomes:

$$\rho\, c_v \frac{\dot{T}}{T} = -\left[\alpha - \frac{1}{E^2}\cdot\frac{\partial E}{\partial T}(\sigma_m + \sigma_a \sin\omega t)\right](\sigma_a\,\omega\cos\omega t). \tag{8}$$

Equation (8) can be integrated as follows:

$$\int_0^t \frac{1}{T}\cdot\frac{\partial T}{\partial t}\,dt = \frac{1}{\rho\, c_v}\int_0^t \left\{\left[-\alpha + \frac{1}{E^2}\cdot\frac{\partial E}{\partial T}\sigma_m\right](\sigma_a\,\omega\cos\omega t) + \left[\frac{1}{E^2}\cdot\frac{\partial E}{\partial T}\cdot\frac{\sigma_a^2\,\omega}{2}\right]\sin 2\,\omega t\right\}dt \tag{9}$$

where the first term on the right side is related to the "first harmonic" (i.e. the harmonic at the frequency ω), and the second term is related to the "second harmonic" (with frequency 2ω).

Integrating both sides of Equation (9), under the assumption that temperature change is small compared with the initial temperature T_o, the expression of $T(t) - T_0$ becomes:

$$T(t) - T_0 = -T_0\frac{\alpha}{\rho\, c_v}\sigma_a \sin\omega t + T_0\frac{1}{\rho\, c_v}\cdot\frac{1}{E^2}\cdot\frac{\partial E}{\partial T}\,\sigma_a\,\sigma_m \sin\omega t + T_0\frac{1}{\rho\, c_v}\cdot\frac{1}{E^2}\cdot\frac{\partial E}{\partial T}\cdot\frac{\sigma_a^2}{2}\sin^2\omega t. \tag{10}$$

2.2.2. Test analytical modelling

The right-hand side of Equation (10) can be reformulated as the sum of three terms:

$$A = -T_0\frac{\alpha}{\rho\, c_v}\sigma_a \sin\omega t = -a\sin\omega t; \tag{11}$$

$$B = T_0\frac{1}{\rho\, c_v}\cdot\frac{1}{E^2}\cdot\frac{\partial E}{\partial T}\,\sigma_a\,\sigma_m \sin\omega t = b\sin\omega t; \tag{12}$$

$$C = T_0\frac{1}{\rho\, c_v}\cdot\frac{1}{E^2}\cdot\frac{\partial E}{\partial T}\cdot\frac{\sigma_a^2}{2}\sin^2\omega t = c\sin^2\omega t. \tag{13}$$

where A corresponds to the first order thermoelastic term, while B and C account for the contribution associated with the change of Young's modulus with the temperature, and a, b and c are the respective amplitudes.

Therefore, Equation (10) can then be written in the form:

$$T(t) - T_0 = A + B + C = -(a-b)\sin\omega t + c\sin^2\omega t. \tag{14}$$

Material parameters α, ρ and c_v of nitinol were imposed based on the literature (Eaton-Evans et al., 2006; Peyroux et al., 1998). The Young's modulus E of the austenite phase was determined from the quasi-static tests described in section 2.1.2. The value of $\partial E/\partial T$ was extracted from the stress-strain curves at 288 K and 293 K (these are in the range of temperature of the presented tests) reported in the study by Tyc et al. on nitinol specimens (Tyc et al., 2020), resulting equal to 440 N/K mm^2. It is important to observe that positive values of $\partial E/\partial T$ imply that the material becomes stiffer as the temperature increases. This behaviour is extremely rare in engineering materials, that typically soften at higher temperatures (for stainless steel $\partial E/\partial T = -19$ N/K mm^2). The parameters describing the thermomechanical response of the material are summarised in Table 1.

$T(t) - T_0$, A, B and C were calculated over time for the different tested conditions, imposing T_0, σ_a, σ_m and ω as in the experiments, and compared with the experimental results. Equation (10) was used to predict the applied stresses (σ_m, σ_a) by fitting the experimental temperature signals with a sum of three sinusoids customised to reproduce the equation terms, imposing the material parameters reported in Table 1. Stresses of each test were also evaluated by imposing in Equation (10) the experimental ratio between the mean and amplitude of the applied stress ($\lambda = \sigma_m/\sigma_a$) and the experimental temperatures at time $t_1 = \pi/2\omega$ and $t_2 = 3\pi/2\omega$.

3. Results and discussion

Phase transformation temperatures, obtained from DSC, resulted equal to 3.3 °C and −16.4 °C for start and finish of austenite-martensite transformation, respectively, and to −8.5 °C ad 5.1 °C for start and finish of martensite-austenite transformation, respectively. Therefore, at the room temperature T_0 the material is in the austenitic phase and exhibits superelastic behaviour.

The engineering stress-strain curve was obtained from the quasi-static test, and linearly fitted to determine the austenite Young's modulus, resulting this equal to 60000 N mm^{-2}.

Strains were calculated from the strain values determined from the DIC analyses performed at 0.02 Hz, at the displacement values achieved at 1 Hz. In fact, as mentioned above, the electrodynamic testing machine did not manage to reach the target displacements at 1 Hz, producing smaller amplitudes. Stress values of the tests at 1 Hz were obtained as the force recorded by the test machine loadcell divided by the initial cross-section.

Table 2 summarises the mean and amplitude of the strains and

Table 1
Material properties.

Material Property	Symbol and Unit	Value
Young's modulus	E [N mm^{-2}]	60000
Material density	ρ [kg mm^{-3}]	6.45×10^{-6}
Coefficient of thermal expansion	α [K^{-1}]	11×10^{-6}
Specific heat at constant volume	c_v [N mm kg^{-1} K^{-1}]	320×10^3
Change of Young's modulus with the temperature	$\partial E/\partial T$ [N K^{-1}mm^{-2}]	440

Table 2
Experimental mean and amplitude strains and stresses and temperatures at time t_1, t_2 for each test.

Test	ε_m, ε_a [%]		σ_m, σ_a [N mm^{-2}]		$T(t_1)$, $T(t_2)$ [K]	
1	0.078	0.023	57.31	19.94	290.603	290.623
2	0.107	0.052	76.24	37.26	290.685	290.705
3	0.134	0.077	93.91	53.09	290.644	290.641
4	0.161	0.104	111.45	69.05	290.706	290.664
5	0.189	0.133	127.59	85.41	290.783	290.692

stresses estimated experimentally for the different tests performed at 1 Hz, with the corresponding temperatures at time t_1, t_2.

The load and temperature waves measured for each test of cyclic loadings are represented in the diagrams on the left column of Fig. 2. Results clearly confirm the unusual response of the material, which exhibits the conventional first order thermoelastic trend, with the temperature variation in opposite-phase to the stress, only for the lowest loading amplitudes (tests 1). At higher load (test 2) a flattening of the troughs in the temperature signal is observed. As load increases (test 3) the temperature signal oscillates at 2 Hz, revealing the dominance of a 2ω modulation (second harmonic). For further increases in the applied load (tests 4 and 5), an in-phase peak of temperature becomes dominant, in agreement with the behaviour reported in previous studies, where austenitic nitinol shows a temperature modulation mainly in phase with the stress (Ahadi et al., 2019; Di Leonardo et al., 2021; Eaton-Evans et al., 2006).

Graphs of the equivalent analytical prediction from Equation (14), drawn for the different test conditions, are represented in the right column of Fig. 2. In particular, to support the interpretation of the phenomenon, the individual contributions of terms A, B and C are reported, clarifying the role of their ratio on the temperature signal modulation. The correspondence between the measurements and the analytical prediction is remarkable, confirming that the higher-order thermoelastic theory (Wong et al., 1987) is adequate to model and interpret the phenomenon. This thermomechanical response is due to the large increase of the austenitic nitinol Young's modulus with the temperature (Eaton-Evans et al., 2006). In fact, the rigidity modulus of common materials changes little with the temperature, slightly reducing as this increases. This implies that terms B and C keep negligible compared to A, and B has the same sign as A. Hence the common behaviour described by the fundamental law of the thermoelastic effect. Instead, the uncommon behaviour of nitinol, only observed in very few materials such as invar (a Fe-Ni alloy) (Özöğüt and Çakır, 2017; Wong et al., 1987), and the large values of $\partial E/\partial T$, greatly increase the contribution of terms B and C to the temperature modulation. These terms become dominant at relatively low stresses, well below phase transformation.

Looking at the studied conditions in more detail, test 1 is characterised by the lowest mean and amplitude load ($\sigma_m = 57$ N mm^{-2}, $\sigma_a = 20$ N mm^{-2}). In this case, the temperature variation is modulated in phase opposition to the stress. As mentioned above, this behaviour is in agreement with the thermoelastic effect observed with common materials, modelled by the fundamental law of the thermoelastic effect described by Equation (5). The analytical graphs show that this behaviour is due to the fact that, in this test condition, a is larger than b and c, and therefore the mean and amplitude of the stress are:

$$\sigma_m < \frac{\alpha E^2}{\frac{\partial E}{\partial T}} \quad \text{and} \quad \sigma_a < \frac{2\alpha E^2}{\frac{\partial E}{\partial T}}. \tag{15}$$

The predominance of term A, which describes the first order thermoelastic effect, causes the temperature wave of test 1 to be in opposite phase to the stress. However, it is important to notice that the compliance with the thermoelastic effect observed in standard materials is only apparent. In fact, the recorded temperature variation is smaller than that predicted from the fundamental law of the thermoelastic effect, modelled by Equation (5) and described by the green dashed curve in the analytical graph. This is due to the presence of term B, which partially counterbalances A. Moreover, term C, with its double frequency, influences the temperature modulation by flattening the troughs and sharpening the crests of the thermal signal waves.

Increasing the load mean and amplitude in test 2 ($\sigma_m = 76$ N mm^{-2}, $\sigma_a = 37$ N mm^{-2}), the negative peaks of the experimental data appear to be cut off or flattened. The analytical solution on the right panel, where noise is absent, explains and clarifies this behaviour. While the first-order thermoelastic effect, described by term A, remains dominant, the difference between a and b reduces, amplifying the effect of the second harmonic, associated with C. This results in an increase in the value of the crest in opposition with the load, and the appearance of a smaller crest in phase with the load.

In test 3 ($\sigma_m = 94$ N mm^{-2}, $\sigma_a = 53$ N mm^{-2}), the second harmonic becomes dominant, and the temperature signal oscillates about sinusoidally at twice the load frequency (2 Hz). The analytical model clarifies that this condition is achieved when a and b become similar, cancelling out. As a result, the temperature signal is mostly regulated by term C, which has frequency $2\,\omega$. This test result is associated with the following conditions:

$$\sigma_m \approx \frac{\alpha E^2}{\frac{\partial E}{\partial T}}. \tag{16}$$

It is worth observing that, in traction-traction cyclic loading (also typical in operating cardiovascular devices), σ_a is always smaller than σ_m, so that c will be always smaller than one quarter of b (see Equations (12) and (13)). As a result, the second harmonic becomes dominant only for a very narrow range of conditions, when a and b are very close to each other. Therefore, this second harmonic condition can be very useful for stress analysis, as it allows to determine the value of the mean and amplitude of the stress. Otherwise, if these are known, it can be used to estimate material properties such as $\partial E/\partial T$.

In test 4 ($\sigma_m = 111$ N mm^{-2}, $\sigma_a = 69$ N mm^{-2}) both the mean and amplitude stress increase, determining a rise in the contribution of B compared to A and, therefore, the in phase crest associated with term B becomes predominant over the in phase opposition peak. Moreover, the difference between b and a still is of the same order as c. This causes the presence of a smaller crest, in phase opposition with the load. The effect is further amplified with the load conditions of test 5 ($\sigma_m = 127$ N mm^{-2}, $\sigma_a = 85$ N mm^{-2}). The resulting thermoelastic signal in phase with the loading wave has been well reported in the literature (Ahadi et al., 2019; Di Leonardo et al., 2021; Eaton-Evans et al., 2006), where the temperature modulation of austenitic nitinol in phase to the stress austenite is well documented. This type of thermal response occurs when b becomes larger than a, at loads:

$$\sigma_m > \frac{\alpha E^2}{\frac{\partial E}{\partial T}}. \tag{17}$$

The above model of the austenitic temperature modulation with the level of stress allows to adopt IRT to identify the regions subjected to higher stress levels. In fact, based on the thermomechanical response (in phase, at double frequency and in phase opposition) and knowing the thermoelastic and mechanical parameters, it is possible to extract the range of stress from Equations (15)–(17).

Moreover, if λ is known, the stress distribution can still be determined from the thermal signal, by solving Equation (10) at time t_1 and t_2:

$$T(t_1) - T_0 = -T_0\frac{\alpha}{\rho\, c_v\, \lambda}\sigma_m + T_0\frac{1}{\rho\, c_v\, \lambda}\cdot\frac{1}{E^2}\cdot\frac{\partial E}{\partial T}{\sigma_m}^2 + T_0\frac{1}{\rho\, c_v\, \lambda^2}\cdot\frac{1}{E^2}\cdot\frac{\partial E}{\partial T}\cdot\frac{{\sigma_m}^2}{2}; \tag{18}$$

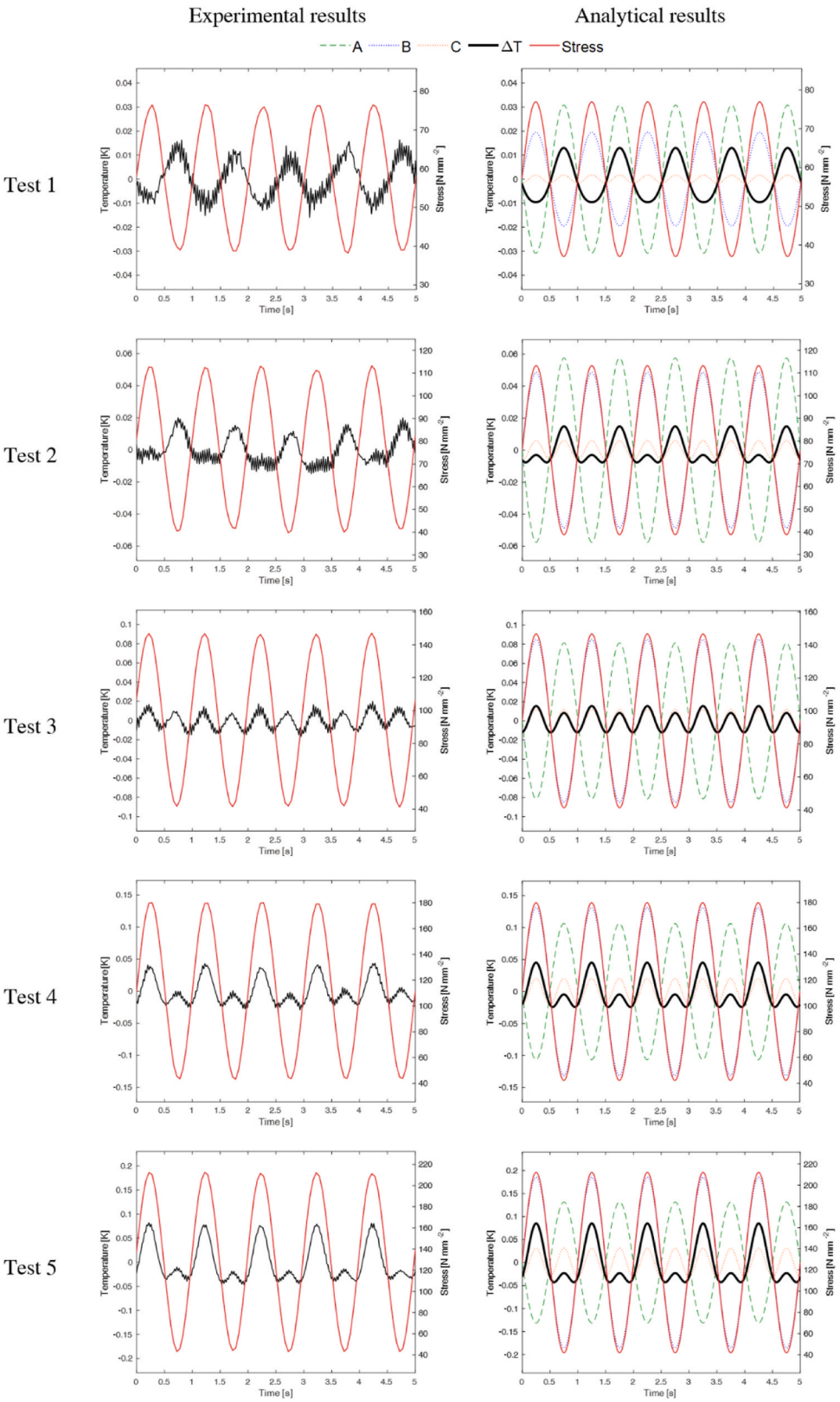

Fig. 2. Experimental and analytical results for each cyclic test. (video 1 in the supplementary material reports the temperature evolution analytically predicted at increasing applied load).

$$T(t_2) - T_0 = T_0 \frac{\alpha}{\rho\, c_v\, \lambda} \sigma_m - T_0 \frac{1}{\rho\, c_v\, \lambda} \cdot \frac{1}{E^2} \cdot \frac{\partial E}{\partial T}\, {\sigma_m}^2 + T_0 \frac{1}{\rho\, c_v\, \lambda^2} \cdot \frac{1}{E^2} \cdot \frac{\partial E}{\partial T} \cdot \frac{{\sigma_m}^2}{2}. \tag{19}$$

Since tests are performed in the linear elastic austenitic region, below the SIMT plateau, proportionality between external and internal actions, displacements and deformations implies that λ can be calculated from any of these quantities (e.g. the applied forces or displacements).

Solving the system of Equations (18) and (19) with respect to σ_m, the mean stress and stress amplitude can be obtained as:

$$\sigma_m = \frac{\alpha + \sqrt{\alpha^2 + 2\frac{1}{E^2}\frac{\partial E}{\partial T}\frac{\rho\, c_v\, \lambda}{T_0}(T(t_1) - T(t_2))}}{\frac{2}{E^2}\frac{\partial E}{\partial T}}; \quad \sigma_a = \frac{\sigma_m}{\lambda}. \tag{20}$$

Table 3 includes the values of σ_m, σ_a estimated from the fitting, as described above and determined by inputting the experimental temperatures $T(t_1)$ and $T(t_2)$ of each test (reported in Table 2) in Equation (20). Comparison of the values obtained from fitting and from the equation with the corresponding quantities measured from the loadcell (in Table 2) indicates that the analytical equation provides more accurate estimates, with maximum percentage difference generally below 5 %, except for Test 1. However, the larger error observed in the first test can be justified by the low stress values and variation applied in this case, which are of the same order of magnitude as the noise in the thermal signal.

Hence, despite the study confirming that the common fundamental law of the thermoelastic effect is inapplicable to study the stress distribution in austenitic nitinol, the use of the higher-order thermoelastic theory overcomes this limit, allowing the application of TSA to extract essential information on the stress state. If the ratio between the mean and amplitude of the applied load is known, the stress values can be determined with satisfactory accuracy.

4. Conclusion

This work analyses, both experimentally and analytically, the thermomechanical response of nitinol in a stable austenitic configuration, under small cyclic loading. This loading configuration is particularly relevant for the assessment of a number of critical applications, including transcatheter medical devices. Results confirm that the material exhibits an unconventional thermomechanical behaviour, with the temperature either in phase opposition or in phase with the stress, in dependence of the load level. The presented study has shown that the higher-order thermoelastic law is an adequate and accurate model, and allows to expand the application of TSA to the assessment of austenitic nitinol, unlike the fundamental law of the standard TSA.

In particular, the formulation applied to a uniaxial test has been shown suitable to obtain the material properties and the regions characterised by higher stress levels. Knowing the ratio between the mean and the amplitude of applied load, the higher-order thermoelastic law also allows to estimate the local stress state with basic equations, extending the applicability of TSA to the evaluation of the local stress levels in loading situations more descriptive of critical operating conditions experienced by nitinol superelastic components.

CRediT authorship contribution statement

V. Pinto: Writing – original draft, Visualization, Validation, Methodology, Investigation, Formal analysis, Data curation, Conceptualization. **S. Di Leonardo:** Writing – original draft, Visualization, Validation, Methodology, Investigation, Formal analysis, Data curation, Conceptualization. **G. Pitarresi:** Writing – review & editing, Visualization, Validation, Supervision, Methodology, Investigation, Formal analysis, Data curation, Conceptualization. **G. Burriesci:** Writing – review & editing, Visualization, Validation, Supervision, Methodology, Investigation, Formal analysis, Data curation, Conceptualization.

Funding

This work was supported by PON R&I 2014/2020, D.M. N. 1061 of August 10, 2021.

Table 3
Mean and amplitude stresses predicted by sinusoidal fitting and calculated by using Equation (20) (departure from experimental values of σ_m and σ_a).

Test	σ_m, σ_a (fitting) [N mm^{-2}]		σ_m, σ_a (20) [N mm^{-2}]	
1	52.02 (−9 %)	15.19 (−24 %)	63.26 (+10 %)	22.20 (+11 %)
2	72.26 (−5 %)	31.52 (−15 %)	74.06 (−3 %)	36.05 (−3 %)
3	92.54 (−1 %)	43.13 (−19 %)	91.81 (−2 %)	51.76 (−3 %)
4	107.99 (−3 %)	64.90 (−6 %)	108.00 (−3 %)	67.14 (−3 %)
5	123.49 (−3 %)	80.58 (−6 %)	122.51 (−4 %)	81.36 (−5 %)

Declaration of competing interest

The authors declare that they have no known competing financial interests or personal relationships that could have appeared to influence the work reported in this paper.

Appendix A. Supplementary data

Supplementary data to this article can be found online at https://doi.org/10.1016/j.mechmat.2025.105506.

Data availability

Data will be made available on request.

References

Ahadi, A., Kawasaki, T., Harjo, S., Ko, W.S., Sun, Q.P., Tsuchiya, K., 2019. Reversible elastocaloric effect at ultra-low temperatures in nanocrystalline shape memory alloys. Acta Mater. 165, 109–117. https://doi.org/10.1016/j.actamat.2018.11.035.
ASTM F2004-03, 2018. ASTM F2004-03 transformation temperature of nickel-titanium alloys by thermal analysis 1. ASTM International 5, 11–14.
Berti, F., Wang, P.J., Spagnoli, A., Pennati, G., Migliavacca, F., Edelman, E.R., Petrini, L., 2021. Nickel–titanium peripheral stents: which is the best criterion for the multiaxial fatigue strength assessment? J. Mech. Behav. Biomed. Mater. 113, 104142. https://doi.org/10.1016/j.jmbbm.2020.104142.
Blaber, J., Adair, B., Antoniou, A., 2015. Ncorr: open-source 2D digital image correlation matlab software. Exp. Mech. 55, 1105–1122. https://doi.org/10.1007/s11340-015-0009-1.
Bonsignore, C., Shamini, A., Duerig, T., 2019. The role of parent phase compliance on the fatigue lifetime of Ni–Ti. Shape Memory and Superelasticity 5, 407–414. https://doi.org/10.1007/s40830-019-00253-2.
Cao, H., Wu, M.H., Zhou, F., McMeeking, R.M., Ritchie, R.O., 2020. The influence of mean strain on the high-cycle fatigue of nitinol with application to medical devices. J. Mech. Phys. Solid. 143. https://doi.org/10.1016/j.jmps.2020.104057.
Chrysochoos, A., 2012a. Thermomechanical analysis of the cyclic behavior of materials. Procedia IUTAM 4, 15–26. https://doi.org/10.1016/j.piutam.2012.05.003.
Chrysochoos, A., 2012b. Thermomechanical analysis of the cyclic behavior of materials. Procedia IUTAM 4, 15–26. https://doi.org/10.1016/j.piutam.2012.05.003.
Chrysochoos, A., Pham, H., Maisonneuve, O., 1996. Energy balance of thermoelastic martensite transformation under stress. Nucl. Eng. Des. 162, 1–12. https://doi.org/10.1016/0029-5493(95)01140-4.
Churchill, C.B., Shaw, J.A., Iadicola, M.A., 2010. Tips and tricks for characterizing shape memory alloy wire: part 4 - thermo-mechanical coupling: experimental characterization of active materials series. Exp. Tech. 34, 63–80. https://doi.org/10.1111/j.1747-1567.2010.00619.x.
Di Leonardo, S., Cappello, R., Burriesci, G., Pitarresi, G., 2021. Investigation of the thermomechanical response of cyclically loaded niti alloys by means of temperature frequency domain analyses. Materials 14. https://doi.org/10.3390/ma14247866.
Eaton-Evans, J., Dulieu-Barton, J.M., Little, E.G., Brown, I.A., 2006. Thermoelastic studies on nitinol stents. J. Strain Anal. Eng. Des. 41, 481–495. https://doi.org/10.1243/03093247JSA195.
Eaton-Evans, J., Dulieu-Barton, J.M., Little, E.G., Brown, I.A., 2008. Observations during mechanical testing of nitinol. Proc Inst Mech Eng C J Mech Eng Sci 222, 97–105. https://doi.org/10.1243/09544062JMES797.
Furgiuele, F., Magarò, P., Maletta, C., Sgambitterra, E., 2020. Functional and structural fatigue of pseudoelastic NiTi: global Vs local thermo-mechanical response. Shape Memory and Superelasticity 6, 242–255. https://doi.org/10.1007/s40830-020-00289-9.
Lagoudas, D.C., 2008. Shape Memory Alloys: Modeling and Engineering Applications. Springer, New York, NY. https://doi.org/10.1007/978-0-387-47685-8.
Launey, M.E., Ong, I., Berg, B.T., Pelton, A.R., 2023. Considerations on tension–tension fatigue predictions for nitinol. Shape Memory and Superelasticity 9, 97–115. https://doi.org/10.1007/s40830-023-00427-z.
Lemaitre, J., Chaboche, J.L., Maji, A.K., 1993. Mechanics of solid materials. J. Eng. Mech. 119, 642–643. https://doi.org/10.1061/(ASCE)0733-9399(1993)119:3(642.2.

Mitchell, M.R., Berg, B.T., Woods, T.O., Jerina, K.L., 2019. Fourth symposium on fatigue and francture of metallic medical materialsand devices. https://doi.org/10.1520/STP1616-EB.

Özöğüt, U.C., Çakır, A., 2017. Investigation of temperature dependent magnetization and elastic modulus in Si-doped Fe65Ni35invar alloys. J. Alloys Compd. 705, 126–130. https://doi.org/10.1016/j.jallcom.2017.02.066.

Petrini, L., Migliavacca, F., 2011. Biomedical applications of shape memory alloys. Journal of Metallurgy 1–15. https://doi.org/10.1155/2011/501483, 2011.

Peyroux, R., Chrysochoos, A., Licht, C., Löbel, M., 1998. Thermomechanical couplings and pseudoelasticity of shape memory alloys. Int. J. Eng. Sci. 36, 489–509. https://doi.org/10.1016/S0020-7225(97)00052-9.

Pieczyska, E.A., Tobushi, H., Kulasinski, K., 2013. Development of transformation bands in TiNi SMA for various stress and strain rates studied by a fast and sensitive infrared camera. Smart Mater. Struct. 22. https://doi.org/10.1088/0964-1726/22/3/035007.

Pinto, V., Cappello, R., Di Leonardo, S., Catalanotti, G., Burriesci, G., Pitarresi, G., 2025. Evaluation of NiTi under low-amplitude cyclic loading by means of thermographic harmonic analysis. Mech. Mater. 206. https://doi.org/10.1016/j.mechmat.2025.105334.

Pitarresi, G., Patterson, E.A., 2003. A review of the general theory of thermoelastic stress analysis. J. Strain Anal. Eng. Des. 38, 405–417. https://doi.org/10.1243/03093240360713469.

Senthilnathan, K., Shamimi, A., Bonsignore, C., Paranjape, H., Duerig, T., 2019. Effect of prestrain on the fatigue life of superelastic nitinol. J. Mater. Eng. Perform. 28, 5946–5958. https://doi.org/10.1007/s11665-019-04334-2.

Song, D., Shi, W., Xu, B., et al., 2026. A thermo-mechanically coupled constitutive model for temperature- and rate-dependent cyclic functional degradation of NiTi shape memory alloys. Acta Mech. Sin. 42, 425060. https://doi.org/10.1007/s10409-025-25060-x.

Soul, H., Yawny, A., 2017. Effect of variable amplitude blocks' ordering on the functional fatigue of superelastic NiTi wires. Shape Memory and Superelasticity 3, 431–442. https://doi.org/10.1007/s40830-017-0126-z.

Tušek, J., Žerovnik, A., Čebron, M., Brojan, M., Žužek, B., Engelbrecht, K., Cadelli, A., 2018. Elastocaloric effect vs fatigue life: exploring the durability limits of Ni-Ti plates under pre-strain conditions for elastocaloric cooling. Acta Mater. 150, 295–307. https://doi.org/10.1016/j.actamat.2018.03.032.

Tyc, O., Heller, L., Vronka, M., Šittner, P., 2020. Effect of temperature on fatigue of superelastic NiTi wires. Int. J. Fatig. 134, 105470. https://doi.org/10.1016/j.ijfatigue.2020.105470.

Tzamtzis, S., Viquerat, J., Yap, J., Mullen, M.J., Burriesci, G., 2013. Numerical analysis of the radial force produced by the Medtronic-CoreValve and Edwards-SAPIEN after transcatheter aortic valve implantation (TAVI). Med. Eng. Phys. 35, 125–130. https://doi.org/10.1016/j.medengphy.2012.04.009.

Wadood, A., 2016. Brief overview on nitinol as biomaterial. Adv. Mater. Sci. Eng. 2016. https://doi.org/10.1155/2016/4173138.

Wolcott, M.P., 1990. Cellular solids: structure and properties. Materials Science and Engineering: a, second ed. Cambridge University Press. https://doi.org/10.1016/0921-5093(90)90295-e.

Wong, A.K., Jones, R., Sparrow, J.G., 1987. Thermoelastic constant or thermoelastic parameter? J. Phys. Chem. Solid. 48, 749–753. https://doi.org/10.1016/0022-3697(87)90071-0.

Xiao, Y., Jiang, D., 2022. Effects of structural geometry on the localized deformation of superelastic NiTi sheets. Int. J. Solid Struct. 257, 111762. https://doi.org/10.1016/j.ijsolstr.2022.111762.

Xie, X., Kan, Q., Kang, G., Li, J., Qiu, B., Yu, C., 2016. Observation on the transformation domains of super-elastic NiTi shape memory alloy and their evolutions during cyclic loading. Smart Mater. Struct. 25. https://doi.org/10.1088/0964-1726/25/4/045003.

Yin, H., Li, M., Sun, Q., 2021. Thermomechanical coupling in cyclic phase transition of shape memory material under periodic Stressing—experiment and modeling. J. Mech. Phys. Solid. 149. https://doi.org/10.1016/j.jmps.2020.104199.

Yu, C., Kang, G., Song, D., Kan, Q., 2015. Effect of martensite reorientation and reorientation-induced plasticity on multiaxial transformation ratchetting of superelastic NiTi shape memory alloy: new consideration in constitutive model. Int. J. Plast. 67, 69–101. https://doi.org/10.1016/j.ijplas.2014.10.001.

Yu, C., Zhou, T., Kan, Q., Kang, G., Fang, D., 2022. A two-scale thermo-mechanically coupled model for anomalous martensite transformation and elastocaloric switching effect of shape memory alloy. J. Mech. Phys. Solid. 164, 104893. https://doi.org/10.1016/j.jmps.2022.104893.

Zhang, Y., Kang, G., Miao, H., Yu, C., 2022. Cyclic degeneration of elastocaloric effect for NiTi shape memory alloy: experimental observation and constitutive model. Int. J. Solid Struct. 248, 111638. https://doi.org/10.1016/j.ijsolstr.2022.111638.

Zhang, K., Li, M., Sun, Q., Zhang, L., Zhou, G., 2024. Interactions among phase transition, heat transfer and austenite plasticity in cyclic compression of NiTi shape memory alloys: effect of loading frequency. J. Mech. Phys. Solid. 191, 105782. https://doi.org/10.1016/j.jmps.2024.105782.

Zheng, L., He, Y., Moumni, Z., 2016. Effects of lüders-like bands on NiTi fatigue behaviors. Int. J. Solid Struct. 83, 28–44. https://doi.org/10.1016/j.ijsolstr.2015.12.021.